On the Interpretation of Complex LEED Patterns

E. Bauer
Michelson Laboratory, China Lake, California 93555

ABSTRACT

A meaningful structure analysis of crystal surfaces has to make use of the dynamical theory of LEED. For surfaces with complex LEED patterns this leads to extremely extensive and costly numerical calculations. Therefore the number of possible surface models to be examined numerically has to be minimized as much as possible. The procedures used in this selection process are discussed from the point of view of general scattering theory. It is concluded that a three-dimensional approach is more appropriate than the two-dimensional approaches used in the past. The interpretation methods are illustrated in the case of the annealed Si(111) surface with 7x7 and $\sqrt{19}$ x $\sqrt{19}$ R(23.5°) pattern. Auger electron spectroscopy is used as the major auxiliary tool in selecting surface models compatible with the LEED patterns.

I. INTRODUCTION

During the past ten years numerous complex LEED patterns have been reported, both for "clean" surfaces and surfaces covered with "adsorption" layers. Most of these patterns--when interpreted at all--were attributed to essentially two-dimensional real superstructures. The interpretation was based on the assumption that the diffraction process is essentially two-dimensional due to the low penetration depth of slow electrons and that the

spot intensity may be analyzed in terms of the elementary theory of LEED. However it was pointed out some time ago [1] and is now widely accepted that the diffraction of slow electrons--as far as the intensities are concerned--must be considered as a three-dimensional process in which the wave field effective in the diffraction process varies strongly normal to the surface (dynamical theory of LEED). It is the purpose of this paper (1) to examine the interpretation of complex LEED patterns from the three-dimensional point of view, and (2) to demonstrate that--in spite of the difficulties in the interpretation of these patterns--surface structures can be determined with a reasonable degree of confidence, if LEED is combined with other techniques, especially Auger electron spectroscopy [2].

II. GENERAL CONSIDERATIONS

The two-dimensional picture of the diffraction process is based on the assumption that the incident wave is attenuated mainly by true absorption, i.e. inelastic scattering. This absorption is assumed to be very strong, so that essentially only those atoms which are directly exposed to the incident wave contribute to the (elastic) diffraction pattern [3]. Conversely, the three-dimensional picture of the diffraction process is based on the assumption that the incident wave--like all diffracted waves--is attenuated mainly by elastic and quasi-elastic scattering. Although the incident wave may be considerably attenuated by scattering in the first atomic layer, the amplitude of the (elastic) wave field incident on the second and following layers still is large because absorption is assumed to be small. Consequently many layers can contribute to the diffraction process. That this picture is at least as reasonable as the previous one follows from calculations [4] of

the absorption and (zero order) scattering coefficients κ and κ_o' respectively, as illustrated in Fig. 1. κ was obtained by treating the crystal as a free electron gas with Fermi momentum $k_F = 1.1$ and with the conduction band bottom 20 eV below the vacuum level in the example shown. κ is determined by the imaginary part $E_I(k)$ of the interaction energy of the incident electron with the electron gas (see e.g. ref. 5):

$$\kappa = \frac{2}{k} E_I(k) = \frac{2}{k} \frac{1}{2\pi^2} \int_{k_F \leq |\underset{\sim}{k}-\underset{\sim}{p}| \leq k} \mathrm{Im} \frac{d\underset{\sim}{p}}{p^2 \epsilon(p, E(k)-E(\underset{\sim}{k}-\underset{\sim}{p})+i\delta)} \qquad (1)$$

$\kappa_o' = \rho Q$ (ρ = number of atoms per unit volume, Q = total elastic atomic scattering cross-section) was calculated by solving the Schroedinger equation for an isolated atom using "trimmed" Thomas-Fermi-Dirac potentials. The "trimming" was done so as to simulate the cut-off of the potential of one atom by that of its neighbor in the solid. Figure 1 clearly shows that attenuation by scattering is about three times as large as by absorption in the energy range of interest, justifying the three-dimensional picture. It has to be kept in mind, however, that in the calculations on which Fig. 1 is based rather crude simplifications were made: (1) the free electron gas approximation is frequently poor and the influence of the surface on $E_I(k)$ [6] has been neglected, and (2) the expression $\kappa_o' = \rho Q$ assumes that no phase relations exist between the waves scattered by the different atoms; in a crystal such phase relations exist and lead to a dependence of κ' on energy and direction of the wave: $\kappa_o' \rightarrow \kappa' = \kappa'(\underline{k})$ (primary extinction).

In the dynamical theory of the diffraction of a plane wave by a plane crystal surface the intensity of a diffracted beam is given by

$$I(\underset{\sim}{k}, \underset{\sim}{k}_o) = |G(\underset{\sim}{k}^t - \underset{\sim}{k}_o^t)|^2 \; |F(\underset{\sim}{k}, \underset{\sim}{k}_o)|^2 \qquad (2)$$

Here $\underset{\sim}{k},\underset{\sim}{k}_o$, $\underset{\sim}{k}^t,\underset{\sim}{k}_o^t$ are the wave vectors of the incident and diffracted waves and their tangential components respectively. The lattice amplitude G determines the geometry of the diffraction pattern and is given by

$$G(\underset{\sim}{k}^t - \underset{\sim}{k}_o^t) = \sum_{m_1 m_2} e^{-i(\underset{\sim}{k}-\underset{\sim}{k}_o)\cdot(m_1\underset{\sim}{c}_1 + m_2\underset{\sim}{c}_2)} \tag{3}$$

where $\underset{\sim}{c}_1$, $\underset{\sim}{c}_2$ represent the lateral periodicity of the true or apparent superstructure of the surface [7]. The dynamical structure amplitude F determines the intensity distribution in the diffraction pattern and is given by

$$F(\underset{\sim}{k},\underset{\sim}{k}_o) = -\frac{1}{4\pi}\int_{\Omega_o} e^{-i\underset{\sim}{k}\cdot\underset{\sim}{r}}\, U(\underset{\sim}{r})\, \psi(\underset{\sim}{k},\underset{\sim}{k}_o,\underset{\sim}{r})\, d\underset{\sim}{r} \tag{4}$$

The integration extends over the whole dynamical unit cell $\Omega_o = (\underset{\sim}{c}_1\underset{\sim}{c}_2\underset{\sim}{c}_3)$ where $\underset{\sim}{c}_3$ ($\perp\underset{\sim}{c}_1,\underset{\sim}{c}_2$) is determined by the penetration depth of the (elastic) electron wave field. U is the effective scattering potential--which generally is complex (absorption!) and energy dependent (exchange, polarization, absorption)--and ψ the wave amplitude. If Ω_o is divided into atomic cells Ω_A (Wigner-Seitz cells) centered at the equilibrium positions $\underset{\sim}{r}$ of the atoms, then F can be written as

$$F = \sum_\nu e^{-i\underset{\sim}{k}\cdot\underset{\sim}{r}_\nu}\cdot\left(-\frac{1}{4\pi}\int_{\Omega_A} e^{-i\underset{\sim}{k}\cdot\underset{\sim}{r}'}\, U(\underset{\sim}{r}_\nu+\underset{\sim}{r}')\, \psi(\underset{\sim}{k},\underset{\sim}{k}_o,\underset{\sim}{r}_\nu+\underset{\sim}{r}')\, d\underset{\sim}{r}'\right). \tag{4a}$$

Expression (4a) is similar to the usual expression for the structure amplitude,

$$F = \sum_\nu f_\nu\, e^{-i(\underset{\sim}{k}-\underset{\sim}{k}_o)\cdot\underset{\sim}{r}_\nu} \tag{5}$$

which is obtained when $\psi(\underset{\sim}{r})$ is written in the form of a Bloch wave: $\psi(\underset{\sim}{k},\underset{\sim}{k}_o\underset{\sim}{r}) = \chi(\underset{\sim}{k},\underset{\sim}{k}_o\underset{\sim}{r})\ e^{i\underset{\sim}{k}_o\cdot\underset{\sim}{r}}$, where $\chi(\underset{\sim}{r})$ has the lateral periodicity of the surface. The dynamical scattering amplitude of the atomic cell ν,

$$f_\nu(\underset{\sim}{k},\underset{\sim}{k}_o) = -\frac{1}{4\pi}\int_{\Omega_A} e^{-i(\underset{\sim}{k}-\underset{\sim}{k}_o)\cdot\underset{\sim}{r}'}\ U(\underset{\sim}{r}_\nu+\underset{\sim}{r}')\ \chi(\underset{\sim}{k},\underset{\sim}{k}_o,\underset{\sim}{r}_\nu+\underset{\sim}{r}')\ d\underset{\sim}{r}' \qquad (6)$$

differs considerably from the scattering amplitude of a free atom--both in the Born and partial wave approximation--because ψ (or χ) depends upon $\underset{\sim}{k},\underset{\sim}{k}_o$, the environment and position of the atom in the crystal. To obtain meaningful values for f_ν, the integral equation

$$\psi(\underset{\sim}{k},\underset{\sim}{k}_o\underset{\sim}{r}) = e^{i\underset{\sim}{k}_o\cdot\underset{\sim}{r}} - \frac{1}{4\pi}\int_{\text{crystal}} \frac{e^{ik|\underset{\sim}{r}-\underset{\sim}{r}'|}}{|\underset{\sim}{r}-\underset{\sim}{r}'|}\ U(\underset{\sim}{r}')\ \psi(\underset{\sim}{k},\underset{\sim}{k}_o,\underset{\sim}{r}')\ d\underset{\sim}{r}' \qquad (7)$$

for ψ or the corresponding Schroedinger equation has to be solved. At present this cannot be done for complex surfaces. To determine the nature of complex surfaces now we must therefore simplify the theory of LEED intensities drastically and/or obtain additional information from other observations such as Auger electron spectroscopy [2].

The simplifications of the theory, which have been made in the past were based on the two-dimensional picture of the diffraction process. The trial-and-error method was used in the intensity analysis of patterns from "clean" elemental semiconductors [8-10], and the Patterson function method in the intensity analysis of patterns of CO and O adsorption layers on Pt and Rh [11]. In the first method it is assumed that all atoms ν which contribute to the diffraction process have the same f_ν. This requires that all atoms have the same χ in Eqn. (6). The second method requires the additional assumption that χ is constant in all atoms contributing to the

diffraction process; otherwise the Fourier transform relationship between structure amplitude and electron density, which is the basis of the Patterson function method, does not exist. It is obvious that both methods represent rather drastic simplifications of the diffraction process and that the surface structures derived with them have to be taken with considerable caution as illustrated by the various structures of elemental semiconductor surfaces deduced with the trial-and-error method [8-10].

In this paper, which is based on the three-dimensional picture of the diffraction process, we make a simplfication which is suggested by experiments on surfaces producing LEED patterns expected from the bulk periodicity ("ideal surfaces"). The intensity versus voltage curves of many of these surfaces show main maxima with average spacings corresponding to the periodicity normal to the surface. This indicates that the contribution of the imaginary part of f_ν--resulting from U and χ in Eq. (6)--to the phase term in Eq. (5) does not change it so drastically as to destroy the third Laue condition completely. Consequently, F and $|F|^2 \sim I$ show some periodicity normal to the surface. The gross features of the intensity versus voltage curves--mainly the existence and average spacing of the main maxima--will therefore be used to obtain information on the periodicity of a surface structure normal to the surface, also in the case of complex diffraction patterns. Another piece of information can be obtained from relative intensities. In pseudo-superstructure patterns, i.e. patterns produced by surfaces covered with a surface layer of different lateral periodicity and/or azimuthal orientation [7], the beams produced by single scattering are frequently stronger than the beams due to multiple scattering. This is expected to happen when the third Laue condition for the surface layer is

approximately fulfilled. Therefore fractional order beams which are very strong at voltages V spaced at intervals ΔV different from those of the integral order beams are usually singly scattered beams from the surface layer and can give information on the lateral periodicity of the surface layer. Thus LEED can provide at present information on the lateral and normal geometrical unit cell dimensions of the surface structure, but not on the number, nature, and distribution of the atoms in the unit cell.

In the past, the nature of the atoms present in a given surface structure had to be deduced from the experimental conditions which led to this structure. Auger electron spectroscopy, originally proposed by Lander [12] and perfected by Harris [13], when combined with LEED [2] permits determination of the nature of the atoms present on the surface. When the Auger electron signal is calibrated the number of atoms can be determined too [2]. However, it has to be kept in mind that the amplitude and width of many Auger transitions depend strongly upon the environment of the atom. Therefore the number of atoms of a given kind per unit cell of a suspected structure can in general be determined only after calibration of the Auger signal on a crystal which is known to have this structure. We will now illustrate these general considerations using two of the best known examples of complex patterns.

III. THE "CLEAN" Si(111) SURFACE

Farnsworth et al. [14] discovered ten years ago two complex diffraction patterns on the Si(111) surface, the Si(111)-7x7 (in short, 7) and the Si(111) - $\sqrt{19}$ x $\sqrt{19}$ R(23.5) (in short, $\sqrt{19}$) patterns shown in Fig. 2. These two patterns have since been reproduced in many laboratories under a wide

variety of conditions and therefore have been generally attributed to clean surfaces. On the other hand, it has been suggested that the patterns may be due to double scattering between the Si substrate and a surface reaction layer with different periodicity and/or orientation [15]. Recently it was proposed [16] that the $\sqrt{19}$ pattern is due to a reconstructed surface layer [8-10] stabilized by an extremely small amount of Ni on the otherwise clean Si surface.

The electron energy spectrum--or more precisely its derivative $\frac{dN(E)}{dE}$ -- from a "clean" Si(111) surface, when measured at low resolution and sensitivity (Fig. 3a) does not show any particular features characteristic of impurities; however at high resolution and sensitivity two peaks can be found in the 40 to 60 eV range; one at 45 eV, one at 57 eV (Fig. 3b). In our apparatus these are the positions of the main peaks of Fe and Ni respectively (as determined by depositing Fe and Ni onto the surface). If the crystal is treated so as to produce a 7 pattern, the Fe peak grows with increasing intensity of the 7 pattern and the Ni peak becomes weaker but never disappears completely. When the crystal is treated to develop the $\sqrt{19}$ pattern, the Fe peak disappears almost completely and the Ni peak grows considerably. This is illustrated in Fig. 4 which shows the height of the Ni Auger signal and of the intensity of one of the fractional order spots (0' in Fig. 6) as a function of quenching (annealing) temperature. The curves do not represent equilibrium conditions because the heating period was only 30 sec which is insufficient to establish equilibrium over the rising part of the curve. The relation between Auger signal and spot intensity, however, is clear. If the crystal is heated to 1000°C, where it

produces a 1x1 pattern, both Fe and Ni peaks have nearly disappeared. Thus, the 7 pattern is definitely connected with the presence of Fe, the $\sqrt{19}$ pattern with the presence of Ni in the surface layer. In what way are now Fe and Ni connected with these two structures? We have to consider the following possibilities:

(1) The Fe and Ni atoms simply sit on top of the unreconstructed Si surface forming a two-dimensional true or apparent superstructure.

(2) They represent a trace impurity stabilizing a true or apparent superstructure made up of Si atoms [16].

(3) They are an essential component of a surface layer which consists of both Si and Fe or Ni respectively and form a true or apparent superstructure.

We will examine now these possibilities by analyzing the geometry and the gross features of the intensities of the diffraction patterns.

The 7 pattern is characterized by the high intensity of those fractional order spots which have the indices $\{40\}$, $\{44\}$ with respect to the various integral order spots characteristic of the unreconstructed surface. This suggests that the pattern is not due to a real superstructure but is due to an apparent one produced by multiple scattering between the Si substrate and a surface layer with $\frac{7}{4}$ the lateral periodicity of the Si(111) surface. The I(V) curves of the $\{40\}$ spots--which are the $\{10\}$ spots of the surface layer--show at normal incidence intensity maxima at the following beam energies: 39.5, 56, 79, 97, 126, 151, 191, 222 eV. Assuming zero inner potential these energies correspond to $\frac{1}{\lambda}$ values of .513, .611, .726, .805, .917, 1.003, 1.128, and 1.217 Å^{-1}. If these maxima of the $I(\frac{1}{\lambda})$ curve

are considered to be the main maxima of a structure periodic normal to the surface with a_3, then a_3 can be obtained from

$$\frac{1}{a_3} = a_3^* = \frac{1}{\lambda_{n+1}} + \sqrt{\frac{1}{\lambda_{n+1}^2} - a_1^{*2}} - \frac{1}{\lambda_n} - \sqrt{\frac{1}{\lambda_n^2} - a_1^{*2}}$$ where a_1^* is the lateral reciprocal periodicity: $a_1^* = \frac{4}{7} a_{1\,Si}^* = \frac{4}{7} \cdot \frac{\sqrt{24}}{3a_{Si}} = .172$ Å^{-1}. With the $\frac{1}{\lambda}$ values given above we obtain a mean value of $a_3^* = .204$ Å^{-1} with a root mean square deviation of .012 Å^{-1} and from these values $a_3 = 4.9 \pm .3$ Å which is definitely incompatible with the periodicity of Si normal to the surface. The diffraction pattern always shows perfect sixfold symmetry, even in the rounded regions of the crystal surface. This is usually a quite reliable indication that the sixfold symmetry is not due to three (two) equivalent structures with twofold (threefold) symmetry. The diffraction pattern has therefore to be due to a hexagonal structure with the basal plane parallel to the Si(111) surface or due to a cubic structure parallel to the Si substrate. In such a cubic structure the three-dimensional reciprocal lattice vectors corresponding to $\underset{\sim}{a}_1^*$ and $\underset{\sim}{a}_3^*$ are $\langle 1\bar{1}0 \rangle$ and $[\bar{1}11]$, $\langle 1\bar{1}0 \rangle$ and [222] or $\frac{1}{3}\langle 22\bar{4} \rangle$ and [111] respectively for the various possible lattices. This corresponds to $\frac{a_3^*}{a_1^*}$ ratios of 1.225, 2.45, and .95 respectively. Clearly, only the first ratio which gives an a-value of a = 8.3 Å is compatible with the ratio $\frac{a_3^*}{a_1^*} = \frac{.204 \pm .012}{.172} = 1.185 \pm .070$ deduced from experiment. For a hexagonal surface we obtain $a = \frac{2}{\sqrt{3} a_1^*} = 6.72$ Å. We now have two possible unit cell dimensions for our surface structure which according to the Auger spectrum must contain both Fe and Si: a primitive cubic cell with a = 8.3 Å and a hexagonal cell with a = 6.72 Å and c = 4.9 ± .3 Å. The choice between

them is based on the assumption that the surface layer is thick enough that it may be considered as a bulk phase. The system Fe-Si contains no cubic phase with a = 8.3 Å, but does have a hexagonal phase, the $Fe_5Si_3(\eta)$ phase, with unit cell dimensions which agree very well with our values: a = 6.727, c = 4.705 or 6.742, c = 4.708 Å [17]. We conclude therefore that a Si(111) surface which produces a 7 pattern is not clean but covered with a surface layer with the unit cell dimensions of Fe_5Si_3 (in short "Fe_5Si_3-structure"). The way the 7 pattern is formed by this surface layer is indicated in Fig. 5. The thickness of this layer and the amount of Fe in it cannot be determined at present. However, the high spot-to-background intensity ratio of a well developed 7 pattern suggests that Fe vacancies or other impurities when present are periodically distributed. It is hoped that future Auger work will allow the determination of layer thickness and Fe content.

The $\sqrt{19}$ structure is more difficult to analyze. None of the "fractional" order beams is distinguished by a high intensity at well defined, approximately equally spaced $\frac{1}{\lambda}$ values. Thus no periodicity normal to the surface can be derived from the diffraction pattern. The intensity of several intense fractional order beams is related to the intensity of the integral order beams. This is a strong indication that the diffraction pattern is due to double scattering between the unreconstructed Si substrate and a surface layer with different periodicity and azimuthal orientation. The diffraction pattern (Fig. 2, 6a) consists of two hexagonal patterns (Fig. 6b) which are rotated ± 23.5° against the basic Si pattern. Any pair of vectors $\underset{\sim}{a}^*_1, \underset{\sim}{a}^*_2$ except those of the Si 1x1 pattern can generate this network by combination with the vectors of the basic Si pattern. The observation that the

relative spot intensities in the rounded regions of the surface are the same as those in the flat regions suggests true hexagonal symmetry of the two-dimensional reciprocal net of the surface layer, thus $|\underset{\sim}{a}^*_1| = |\underset{\sim}{a}^*_2| = a^*_1$ and $\sphericalangle(\underset{\sim}{a}^*_1, \underset{\sim}{a}^*_2) = 60°$. The general aspects of the intensity distribution lead to the choice of $\underset{\sim}{a}^*$ vectors $\underset{\sim}{h}_{hk}$ leading to one of the six points (hk) shown in Fig. 6b. In a previous short communication [18], we suggested that $\underset{\sim}{a}^*_1 = \underset{\sim}{h}_{23}$ ($|\underset{\sim}{h}_{23}| = |\underset{\sim}{h}_{32}| = |\underset{\sim}{a}^*_{1\ Si}|$). This suggestion was based on the hypothesis that the surface layer has to have a structure known to occur in the system Ni-Si, a condition which is fulfilled only when $|\underset{\sim}{a}^*_1| = |\underset{\sim}{h}_{23}| = |\underset{\sim}{a}^*_{1\ Si}|$. Two structures, θ-Ni_2Si and $NiSi_2$, when slightly distorted, are then compatible with the geometry of the diffraction patterns. The high temperature (θ) modification of Ni_2Si is hexagonal with a = 3.805 Å and c = 4.890 Å [19]; when its (001) plane is parallel to the substrate, then $|\underset{\sim}{a}^*_1| = \frac{2}{\sqrt{3}a} = .3035$ Å^{-1} which differs 1% from $|\underset{\sim}{a}^*_{1\ Si}| = \frac{\sqrt{24}}{3a_{Si}} = .3007$ Å^{-1}. $NiSi_2$ is cubic with a = 5.395 Å [20]; when present in parallel orientation on the Si(111) surface $|\underset{\sim}{a}^*_1| = .3027$ Å^{-1} which differs only .7% from $|\underset{\sim}{a}^*_{1\ Si}|$. A distinction between these two structures is possible on the basis of the following observations made on Si(111) surfaces producing a 1x1 pattern:

(1) The 1x1 pattern can be obtained in various ways, e.g.: (a) by deposition of Ni to a thickness of several to many atomic layers followed by a short anneal of the crystal at 700°C or lower (surface A), and (b) by annealing of a "clean" crystal for several minutes at 700°C after it had been heated sufficiently long at 1200 to 1300°C to desorb most of the Fe from crystal and leads (surface B).

(2) The surface A is characterized by a strong Ni Auger peak (Fig. 7d), the Ni Auger peak of the surface B is barely detectable.

(3) The $I_{oo}(V)$ curves of both surfaces generally have maxima at nearly the same voltages (or $\frac{1}{\lambda}$ values). The $\frac{1}{\lambda}$ intervals between the main maxima agree in both cases qualitatively with the periodicity of $Si(NiSi_2)$ normal to the surface. However there are significant differences in the relative height of the maxima. In particular, the peak which occurs on surface A at 177 eV is very strong, while the corresponding peak at 181 eV of surface B is very weak.

(4) The spot-to-background intensity ratio of surface A is lower than that of surface B, the Kikuchi pattern of surface A is sharper than that of surface B.

From (2) we conclude that the surface A has a high Ni content, from (3) that its periodicity normal to the surface is essentially the same as that of Si in spite of the high Ni content, and from (4) that the Ni atoms are distributed not at random but in a well ordered manner. An epitaxial surface layer of $NiSi_2$ is the simplest explanation compatible with the conclusions. Unless we invoke the assumption that $NiSi_2$ can grow in two different orientations on the Si(111) surface, e.g. depending upon cooling conditions or impurity effects, we are left with θ-Ni_2Si as the cause of the $\sqrt{19}$ pattern.

It must be kept in mind, however, that θ-Ni_2Si and $NiSi_2$ were selected as possible causes of the $\sqrt{19}$ pattern on the assumption that the surface layer has to have a structure found in bulk. If we drop this assumption the other points (hk) shown in Fig. 6b have to be considered too. We can reduce the number of possible $\underset{\sim}{a}_1^*$ vectors by extracting more information from the LEED pattern. This can be done when the strongly simplifying assumption is made, that the multiple scattering process may be separated into subsequent scattering acts in surface layer and substrate. Then the observed

intensity of a doubly scattered beam should be proportional to the intensity of the substrate beam which produces the doubly scattered beam on its way out through the surface layer. One characteristic feature of the $\sqrt{19}$ pattern is that the intensities of the spots marked A'(B') in Fig. 6a increase and decrease with that of the basic Si spots marked A(B). According to the simplified picture of the double scattering process this can happen only if $\underset{\sim}{a}_1^* = \underset{\sim}{h}_{22}$, $\underset{\sim}{h}_{41}$ or $\underset{\sim}{h}_{33}$, which can be seen by superimposing the corresponding hexagonal networks--such as the one shown in Fig. 6c--with that of the unreconstructed Si surface, using points A and B as origins. Another characteristic feature of the $\sqrt{19}$ pattern is that the spots marked 0' in Fig. 6a are very strong over wide voltage ranges, while the spots 0", 0"' never are very strong. For the chosen $\underset{\sim}{a}_1^*$'s ($\underset{\sim}{h}_{22}$, $\underset{\sim}{h}_{41}$ and $\underset{\sim}{h}_{33}$) these 0 spots (0', 0", and 0'" respectively) are produced by the incident beam and by the 00 beam on its way out through the surface layer and are therefore expected to be strong, leading to the choice of $\underset{\sim}{a}_1^* = \underset{\sim}{h}_{22}$, $|\underset{\sim}{a}_1^*| = \sqrt{\frac{12}{19}}\,|\underset{\sim}{a}_{1\ \mathrm{Si}}^*| = .239$ Å^{-1}. Nothing can be deduced about $|\underset{\sim}{a}_3^*|$ because of the lack of regularity in the I(V) curves due to the strong dynamical coupling between the various beams. Thus we can say only that the surface layer has either a cubic structure with $a = \frac{\sqrt{2}}{|\underset{\sim}{a}_1^*|} = 5.92$ Å or $a = \frac{\frac{1}{3}\sqrt{24}}{|\underset{\sim}{a}_1^*|} = 6.83$ Å or a hexagonal structure with $a = \frac{2}{\sqrt{3}\,|\underset{\sim}{a}_1^*|}$ = 4.83 Å. None of those structures is known to exist in the system Ni-Si. We can therefore only speculate about its nature: it could be an expanded surface layer of Ni_3Si which does not have the structure found in the bulk, but Fe_3Si structure ($a_{Fe_3Si} = 5.64$ Å); or more likely it could contain besides Ni other impurities which determine the structure. This second possibility can by no means be excluded at present, even in the case of the 7 pattern, for the

following reason: most of the Auger electron spectra were obtained with primary energies up to 600 eV. In order to excite an Auger transition efficiently the energy of the incident electrons must be about three times the energy of the lower x-ray level involved in the transition. Consequently, one can detect efficiently only those atoms which have major Auger transitions below 200 to 300 eV. For example the Auger transitions of Ta in this energy region are much weaker than the 45 and 57 eV peaks of Fe and Ni respectively. If present in the surface layer in a state similar to that of Ni, Ta could not be detected at present. A surface layer of composition Ta_2Ni_3Si is therefore not incompatible with the Auger electron spectrum. This composition--like similar ones involving Nb, Mo or W in place of Ta--is hexagonal with $a \approx 4.8$ Å [21,22] which agrees well with the value a = 4.83 Å deduced from the LEED pattern. The observation that the $\sqrt{19}$ pattern forms much faster near the Ta leads than in the center of the crystal is also in favor of such an interpretation.

The results derived above, i.e. (1) a Fe-containing surface layer with Fe_5Si_3 structure as cause of the 7-pattern, and (2) a Ni-containing surface layer with θ-Ni_2Si or Ta_2Ni_3Si structure or with an unknown structure as cause of the $\sqrt{19}$ pattern, lead immediately to a number of questions:

(1) Why do the surface layers have the observed structures and not other structures, e.g., why does Ni not form the $NiSi_2$ (1x1) structure with its low mismatch?

(2) Where is the Fe and Ni coming from?

(3) Why does the Fe-containing layer form at the low temperature, the Ni-containing layer at the higher temperatures?

We have at present no answer to question (1) except the suggestion that the observed structures may have electron configurations leading to a lower surface energy. In the case of the Ni_2Si layer model, the tendency to form Ni_2Si might be attributed to the fact that Ni_2Si has the highest heat of formation in the system Ni-Si [23]. The source for the Fe and Ni may be (a) the interior of the crystal, (b) the crystal mounting, (c) the surface preparation process, (d) the handling of the crystal, and (e) the vacuum system itself. We can exclude (a) as a general source because of the wide variety of high purity crystals which have been investigated. The crystal mounting, usually made of refractory metals like Ta or Mo, may contain a considerable amount of Ni and Fe, e.g., Fansteel metallurgical grade Ta sheet contains up to .02% Fe, and is therefore a likely source in many cases. The acids used in surface preparation contain up to 10^{-3}% Fe which can lead to $2.4 \cdot 10^{15}$ adsorbed Fe atoms on the surface [24], enough to form a Fe_5Si_3 layer one unit cell thick. Variations in surface preparation procedures make this also an unlikely general source. Introduction of Ni into the crystal by improper handling with metal tweezers has already been pointed out [16]. The vacuum system, usually made of stainless steel, or at least containing Fe and Ni parts (e.g., Kovar), can be a continuous source of Fe and Ni via the following process: CO, which is one of the main residual gas components, interacts with Fe(Ni) surfaces to form a Fe(Ni) carbonyl layer. The adsorbed carbonyl molecules can be desorbed either thermally or by collisions of atoms, ions or electrons with the surface. When they hit the surface of the Si crystal or of the crystal mounting they can dissociate depending upon surface condition and temperature leaving

Fe(Ni) on the surface. We believe this process to be the major source in many of our experiments; without it the regeneration of the Fe_5Si_3 structure (with the accompanying Fe Auger Peak) after excessive heating to desorb all Fe would be difficult to understand.

The occurrence of the Fe(Ni)-containing layer at the lower (higher) temperature can be attributed to the relative solid solubilities of Fe and Ni. The solid solubilities of Fe and Ni in Si at 900°C are $6 \cdot 10^{12}$ and $3 \cdot 10^{16}$ atoms/cm^3, respectively; at 1300°C $5 \cdot 10^{16}$ and $8 \cdot 10^{17}$ atoms/cm^3, respectively [25,26]. Consequently, when Fe and Ni are supplied simultaneously to the crystal, either by diffusion from the crystal mounting or by carbonyl decomposition, most of the Fe has to stay at the surface in the form of Fe or an Fe-silicide while a considerable amount of Ni can go into solid solution. In particular, at the low annealing temperatures used to produce the 7-pattern essentially all Fe remains at the surface, thus forming the 7 pattern. (A Fe_5Si_3 layer 1 unit cell thick contains $2.5 \cdot 10^{15}$ Fe atoms/cm^2.) In order to produce the $\sqrt{19}$ pattern the Fe has to be desorbed or dissolved in the bulk of the crystal or in the crystal mounting and replaced by a sufficient amount of Ni. This requires first that the crystal is heated high enough, e.g., to 1000°C, where the vapor pressure of Fe is $5 \cdot 10^{-7}$ torr so that desorption becomes possible, or that Fe can diffuse into the crystal mounting. Significant dissolution in the bulk of the Si crystal is only possible at higher temperatures; for example, dissolution of the Fe contained in a Fe_5Si_3 layer one unit cell thick can occur only at temperatures above 1180°C. However, if the crystal contains precipitation centers at which Fe can precipitate out, the crystal itself can also act as a sink for Fe. The second prerequisite for the production

of the $\sqrt{19}$ pattern is proper pretreatment of the crystal (and/or crystal mount) such that it contains a sufficient amount of dissolved or precipitated Ni, which can dissolve at the annealing temperature, e.g. at 1000°C where the saturation concentration is $1.5 \cdot 10^{17}$ Ni atoms/cm^3 [26]. Upon rapid cooling some of the Ni can then precipitate out at the surface to form the $\sqrt{19}$ structure. These considerations show that the formation of the observed surface layers depends upon many parameters. This is probably to a large extent responsible for the differences between the required annealing conditions as found in various laboratories [8;13,16,27].

SUMMARY

In this paper we have proposed a view of the diffraction process which is diametrically opposite to that which has been the basis of the methods used in the past to interpret complex LEED pattern. Then absorption was assumed to be so strong that an essentially two-dimensional structure analysis could be made. Here absorption is considered to be so weak that the elastic wave field can penetrate considerably into the crystal and a three-dimensional approach appears more appropriate. We have applied this approach to the problem of the annealed Si(111) plane, not so much to come up with unequivocal structures; rather, we wanted to illustrate the procedures which can be followed to arrive at surface models which have to be considered in a detailed dynamical structure analysis with numerical methods. More detailed studies should allow reduction of the number of likely surface models still more. For example, Auger electron spectroscopy studies as a function of primary energy at fixed angle of incidence and vice versa which are in progress are expected to give information on the distribution of Fe

and Ni normal to the surface. Increased sensitivity should allow detection of atoms with weaker Auger peaks, e.g, of Ta. A better understanding of the Auger transition probabilities as a function of environment should allow one to obtain information on the area concentration of impurities and their environment. Quantitative studies of the formation kinetics of the various LEED patterns on crystals with controlled impurity and imperfection content also promises to be a useful tool. In conclusion, much experimental work needs to be done before a mathematical structure analysis should be attempted.

ACKNOWLEDGMENT

The author wishes to thank Dr. J. O. Porteus for critically reading the manuscript and for valuable comments. Financial support of the National Aeronautics and Space Administration under Contract No. R-05-030-001 is appreciated.

REFERENCES

[1] E. Bauer, Phys. Rev. 123, 1206 (1961).

[2] R. E. Weber and W. T. Peria, J. Appl. Phys. 38, 4355 (1967).

[3] J. J. Lander, Progr. Solid State Chem. 2, 26 (1965).

[4] H. N. Browne and E. Bauer, unpublished.

[5] J. J. Quinn, Phys. Rev. 126, 1453 (1962).

[6] P. A. Fedders, Phys. Rev. 153, 438 (1967).

[7] E. Bauer, Surface Sci. 7, 351 (1967).

[8] J. J. Lander and J. Morrison, J. Chem. Phys. 37, 729 (1962); J. Appl. Phys. 34, 1403 (1963).

[9] R. Seiwatz, Surface Sci. 2, 473 (1964).

[10] N. R. Hansen and D. Haneman, Surface Sci. 2, 566 (1964).

[11] C. W. Tucker, Jr., Surface Sci. 2, 516 (1964); J. Appl. Phys. 37, 3013, 4147 (1966).

[12] J. J. Lander, Phys. Rev. 91, 1382 (1953).

[13] L. A. Harris, G. E. Res. Develop. Rept. #67C201 (1967); J. Appl. Phys. 39, 1419 (1968).

[14] R. E. Schlier and H. E. Farnsworth, J. Chem. Phys. 30, 917 (1959).

[15] E. Bauer, Colloque Internat. CNRS 1965, No. 152, p. 19.

[16] A. J. van Bommel and F. Meyer, Surface Sci. 8, 467 (1967).

[17] A. R. Weill, Nature 152, 413 (1943).

[18] E. Bauer, Phys. Letters 26, 530 (1968).

[19] K. Toman, Acta Cryst. 5, 329 (1952).

[20] K. Schubert and H. Pfisterer, Z. Metallk. 41, 433 (1950).

[21] D. I. Bardos, K. P. Gupta and P. A. Beck, Trans. Met. Soc. AIME 221, 1087 (1961).

REFERENCES (CONT'D)

[22] M. Yu. Teslyuk, V. Ya. Markiv, and E. I. Gladyshevskii, J. Struct. Chem. 5, 364 (1964).

[23] U. Dehlinger, Z. Metallk. 43, 109 (1952).

[24] V. S. Sotnikov and A. S. Belanovskii, Russ. J. Phys. Chem. 34, 1001 (1960).

[25] J. D. Struthers, J. Appl. Phys. 27, 1560 (1956).

[26] J. H. Aalberts and M. L. Verheijke, Appl. Phys. Letters 1, 19 (1962).

[27] F. Jona, Appl. Phys. Letters 6, 205 (1965); IBM J. Res. Develop. 9, 375 (1965).

FIGURE CAPTIONS

Fig. 1. Attenuation of slow electrons in idealized solids. κ_o' is the scattering coefficient of a hypothetical random distribution of atoms with bulk density and Thomas-Fermi-Dirac potentials "trimmed" to the nearest neighbor distance in the crystal. κ is the absorption coefficient of a free electron gas. $\bar{\Lambda}$ is the mean free path. κ_o' and κ are in atomic units, $\bar{\Lambda}$ in Å.

Fig. 2. LEED patterns from annealed Si(111) planes; (a) 7x7 pattern (80 eV), (b) $\sqrt{19}$ x $\sqrt{19}$ R(23.5°) pattern (55 eV).

Fig. 3. Derivative $\frac{dN(E)}{dE}$ of the total energy distribution of electrons from a Si(111) surface bombarded with slow electrons; (a) total spectrum at low resolution (300 eV primary electrons), numbers on left denote detector sensitivity, numbers on right energy loss values, (b) section of spectrum at high resolution (600 eV primary electrons).

Fig. 4. Amplitude of Auger signal at 56 eV (full circles) and of fractional order spot intensity (open circles) in $\sqrt{19}$ as a function of quenching temperature for 30 sec annealing periods.

Fig. 5. Explanation of 7 pattern in terms of multiple scattering between a surface layer with Fe_5Si_3 unit cell dimensions and the unreconstructed Si substrate; (a) basic Si pattern, (b) Fe_5Si_3 pattern, (c) multiple scattering pattern from superimposed Fe_5Si_3 and Si.

Fig. 6. Analysis of $\sqrt{19}$ pattern. The observed pattern (a) consists of two equivalent patterns (b), which are produced by multiple scattering between the substrate and a surface layer of different orientation and/or periodicity, e.g. like that producing pattern (c).

Fig. 7. Partial energy spectrum of Si(111) surfaces; (a) at 1000°C (1x1 pattern), (b) after quenching to room temperature ($\sqrt{19}$ pattern), (c) after deposition of Ni (LEED only background), (d) after short anneal at 700°C (1x1 pattern).

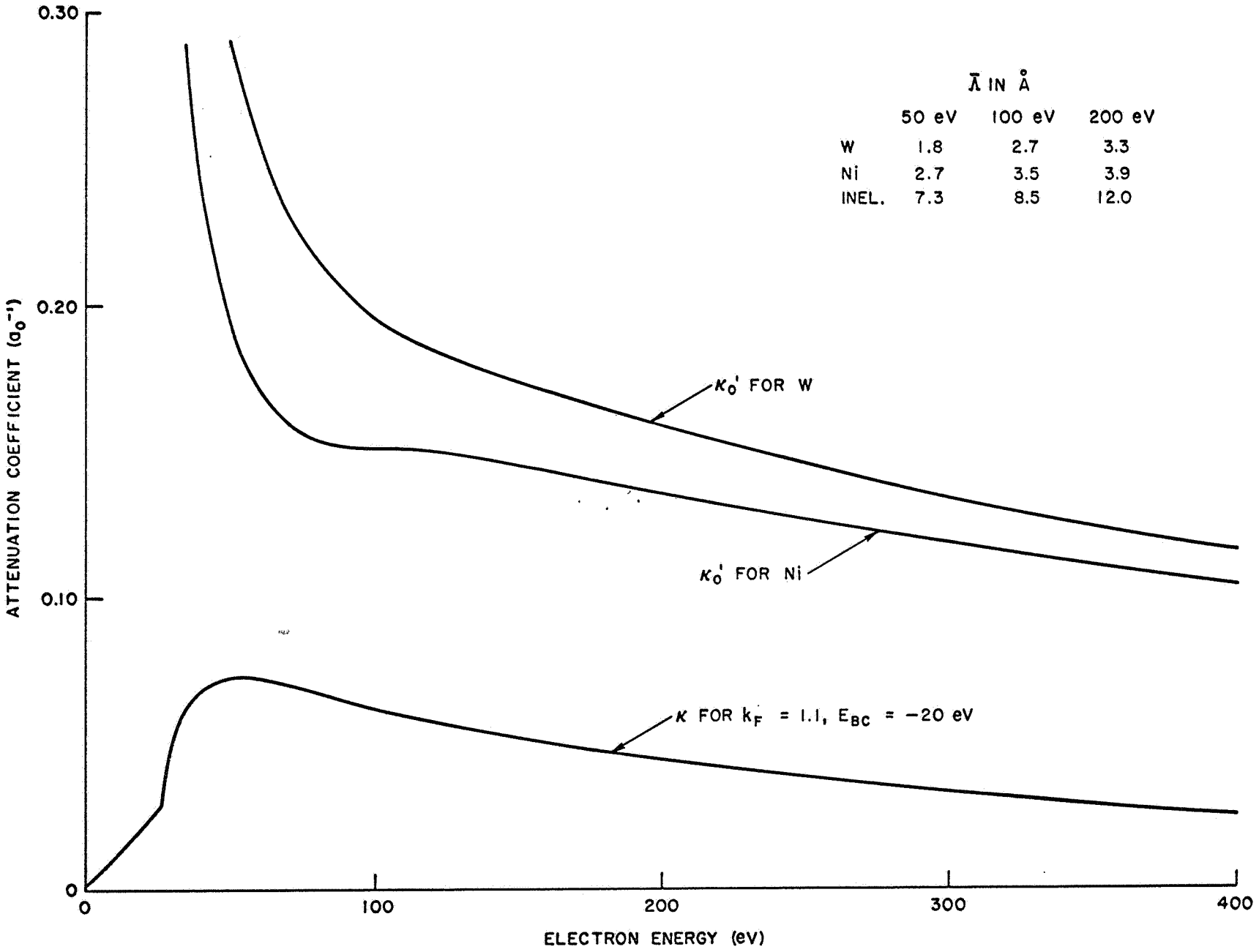
$\bar{\Lambda}$ IN Å
50 eV 100 eV 200 eV
W 1.8 2.7 3.3
Ni 2.7 3.5 3.9
INEL. 7.3 8.5 12.0
K_0' FOR W
K_0' FOR Ni
K FOR k_F = 1.1, E_{BC} = −20 eV
ATTENUATION COEFFICIENT (a_0^{-1})
0.30
0.20
0.10
0
0
100
200
300
400
ELECTRON ENERGY (eV)

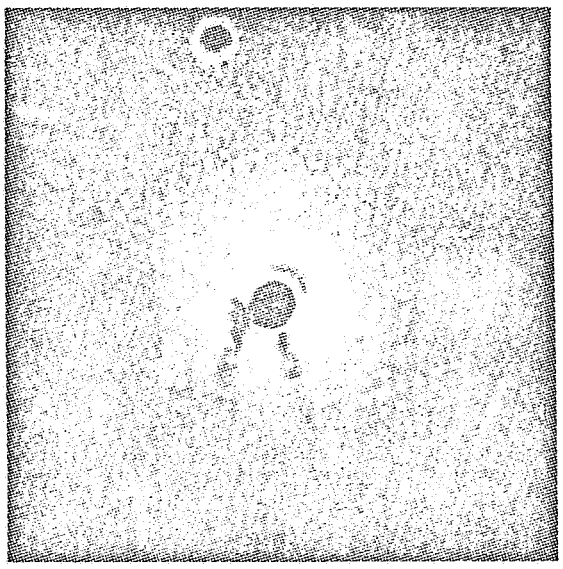

a

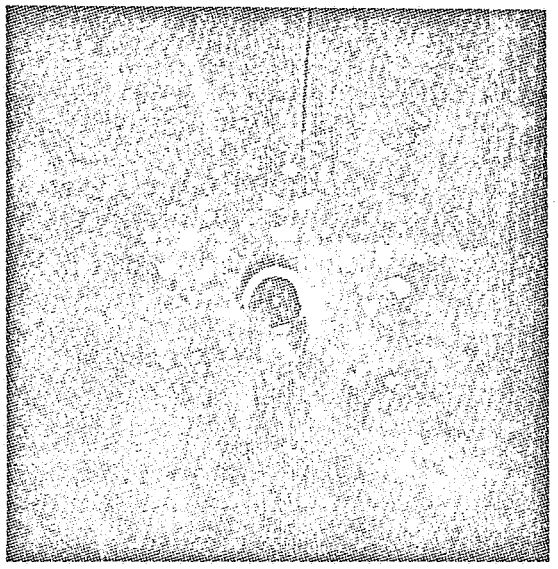

b

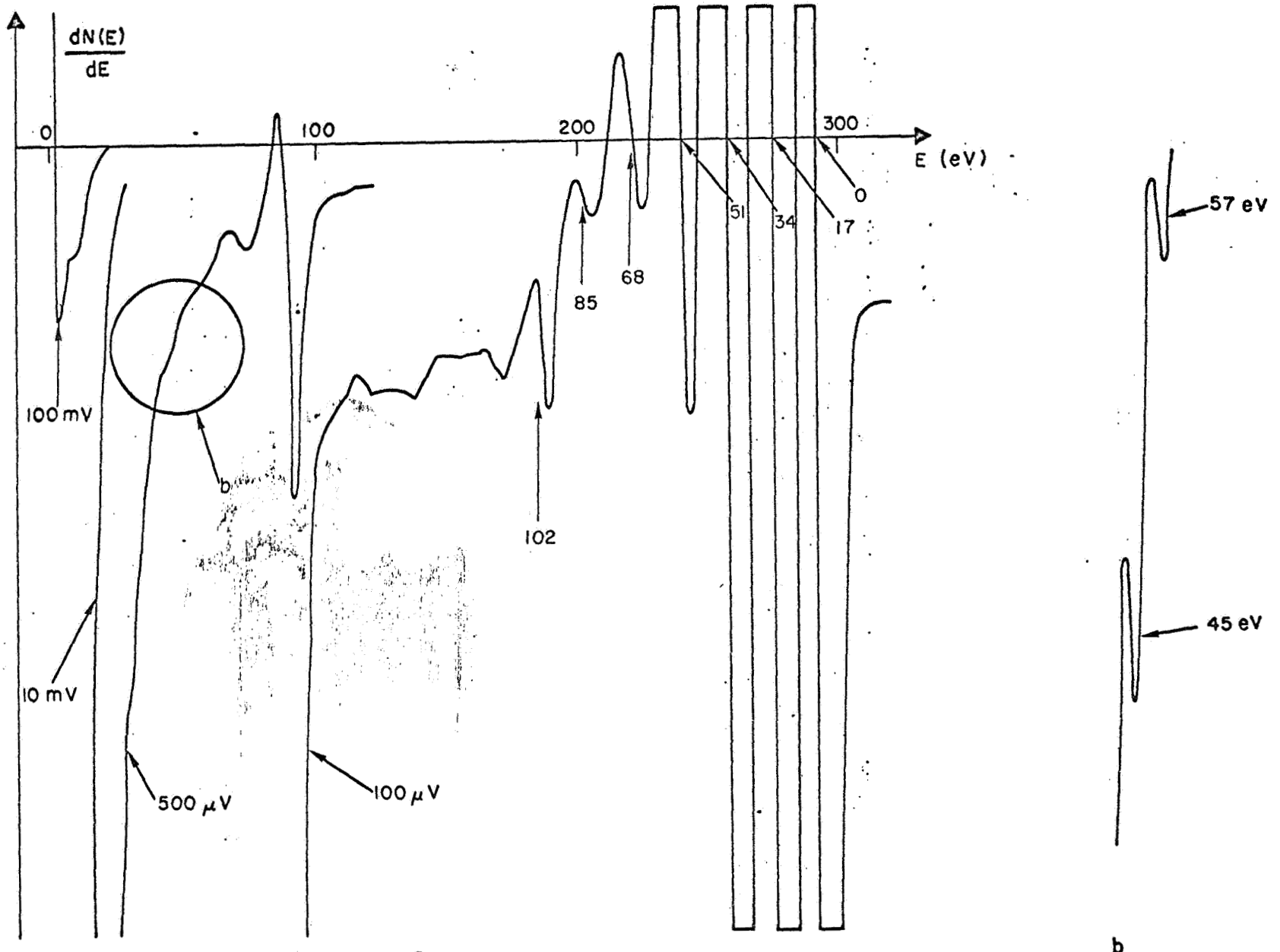
dN(E)
dE
0
100
200
300
E (eV)
0
17
34
51
68
85
102
100 mV
10 mV
500 μV
100 μV
b

a

57 eV
45 eV

b

Fig 5

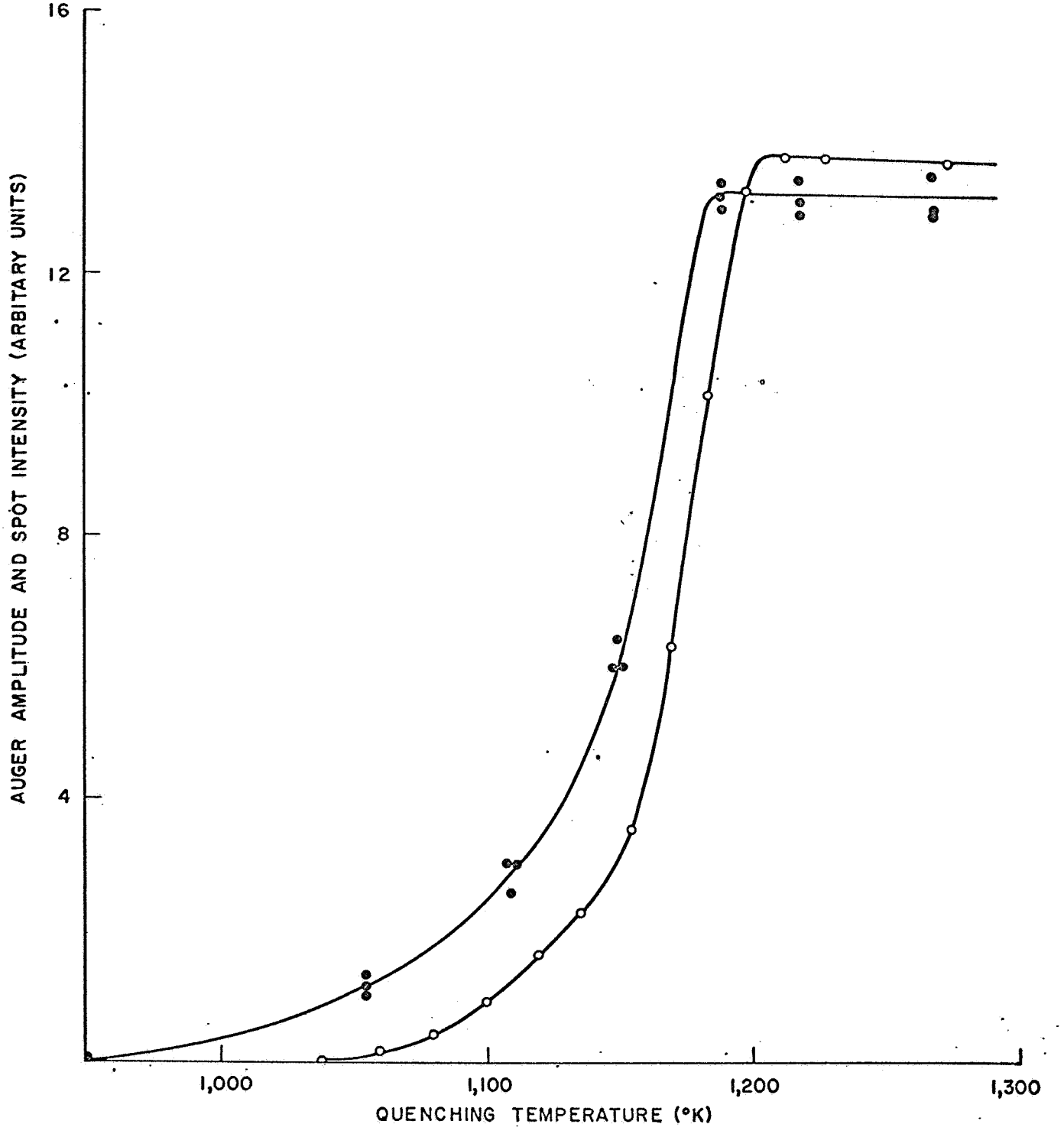
16
12
8
4
AUGER AMPLITUDE AND SPOT INTENSITY (ARBITARY UNITS)
1,000
1,100
1,200
1,300
QUENCHING TEMPERATURE (°K)

Fig. 4.

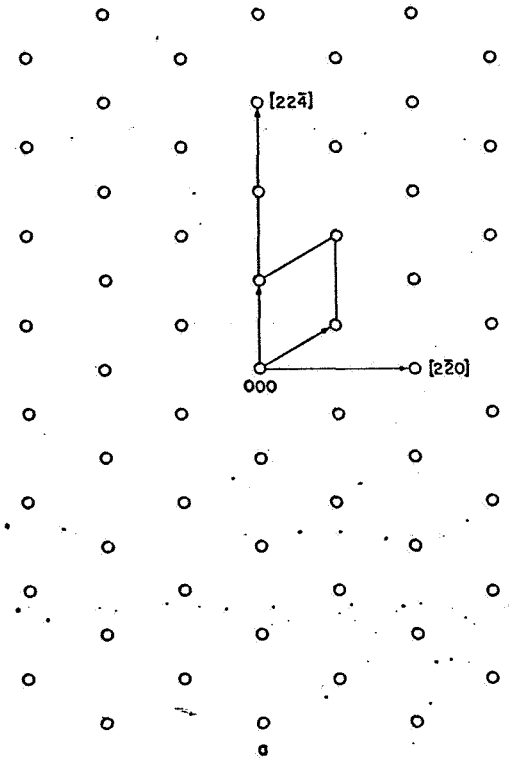

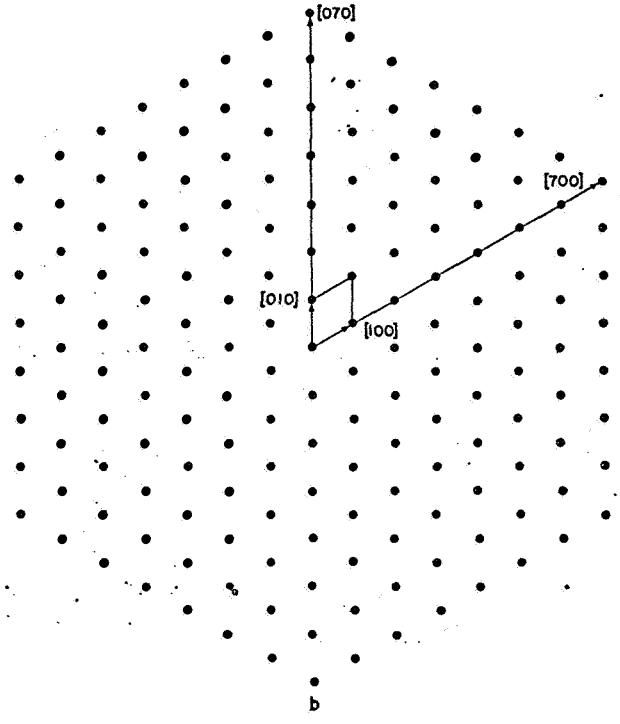

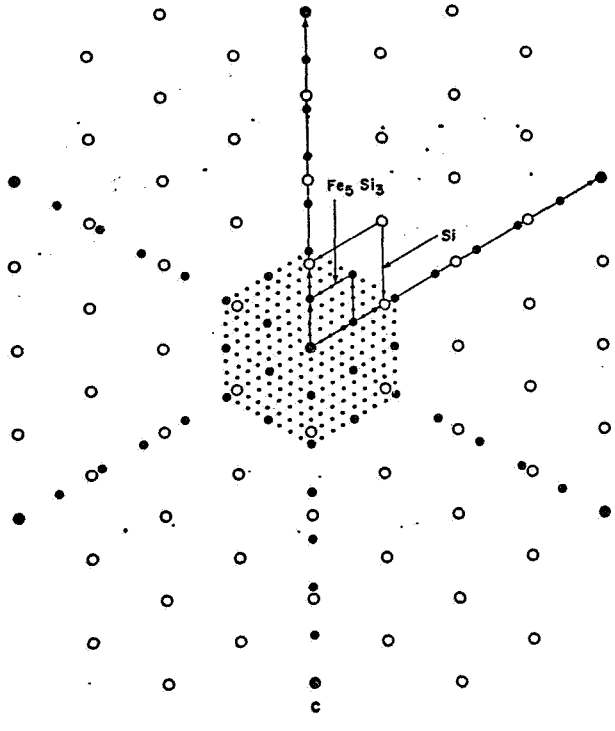

Fig. 5

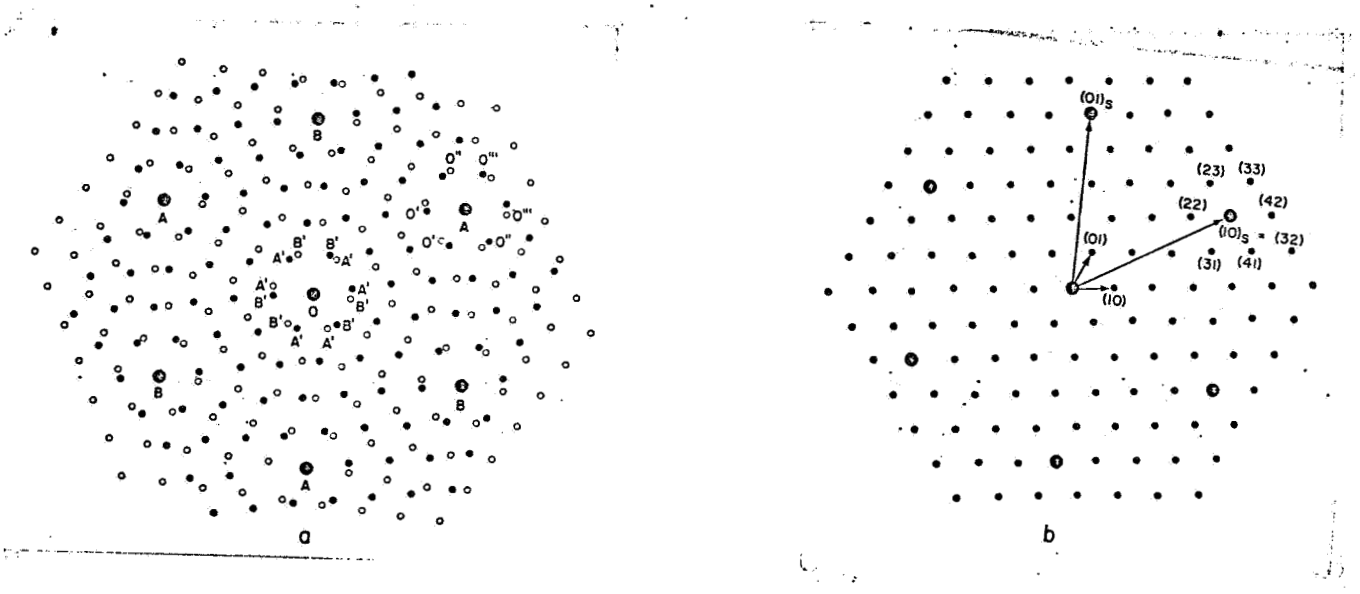

Fig 6

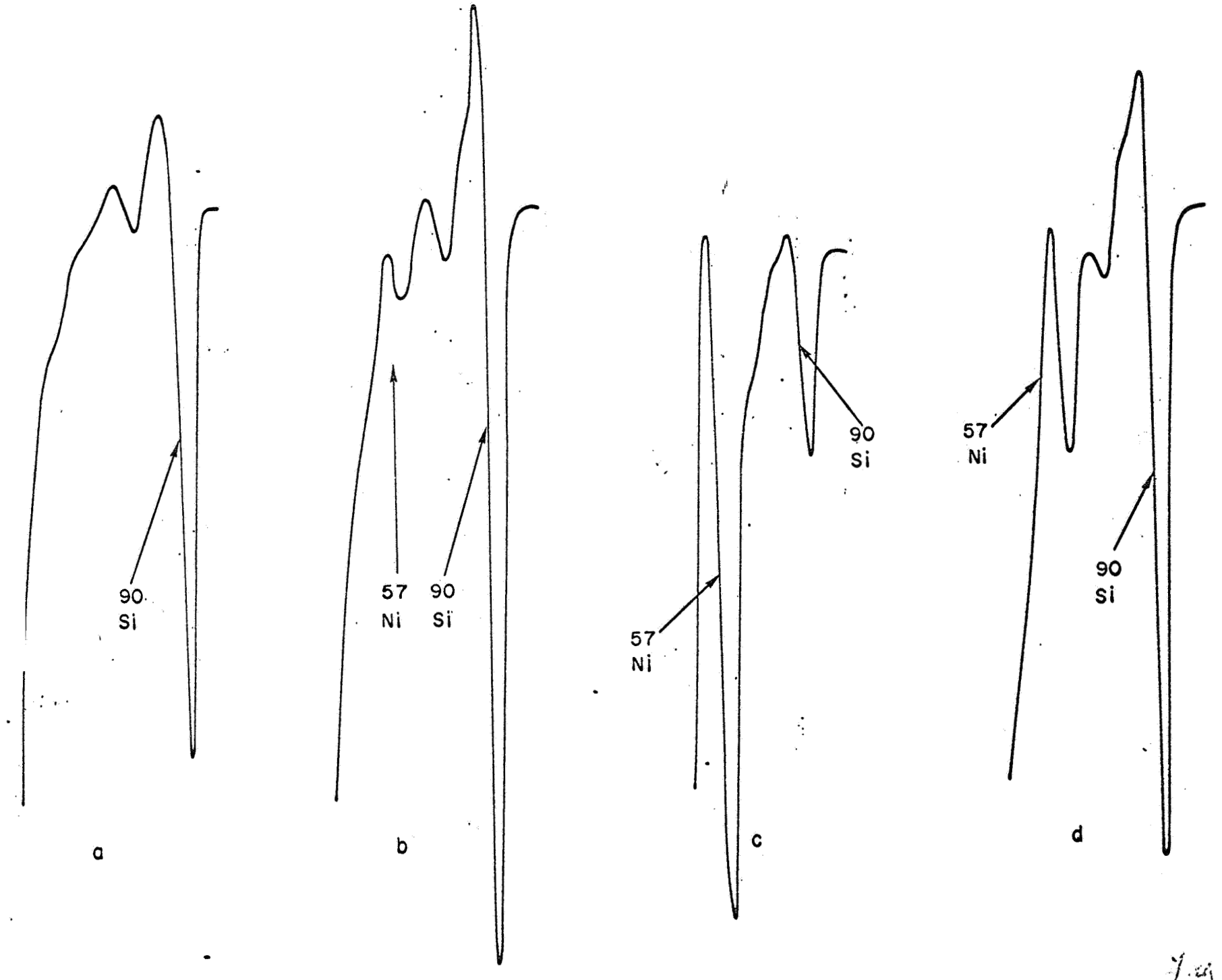

Fig. 7